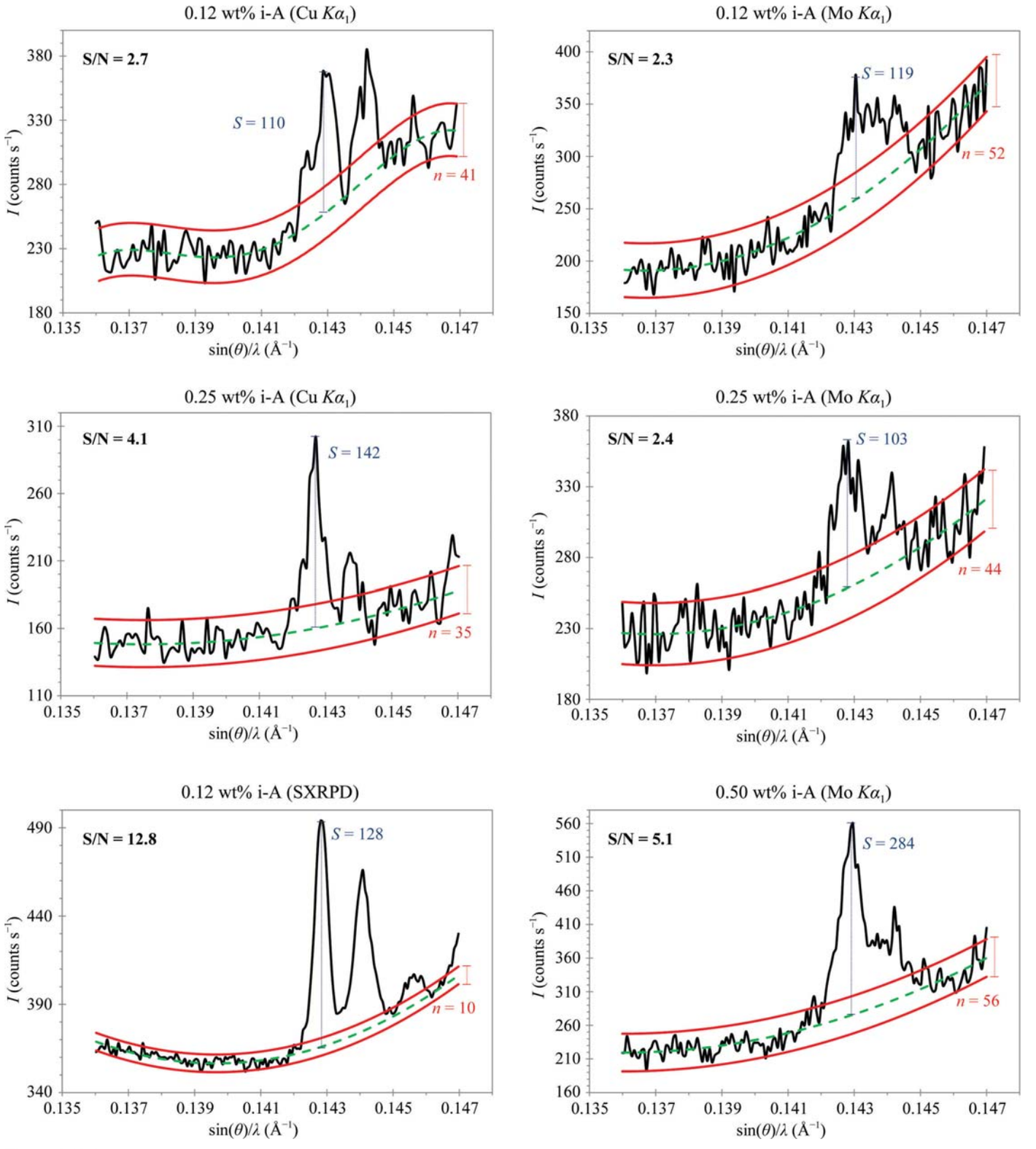

Figure 3.10.4
Selected region of the powder patterns showing the main diffraction peak of insoluble anhydrite for the low-content samples to investigate the limit of detection. Top left: Cu $K\alpha_1$ pattern for CGpQ_0.12A. Middle left, Cu $K\alpha_1$ pattern for CGpQ_0.25A. Bottom left, SXRPD pattern for CGpQ_0.12A. Top right, Mo $K\alpha_1$ pattern for CGpQ_0.12A. Middle right, Mo $K\alpha_1$ pattern for CGpQ_0.25A. Bottom right, Mo $K\alpha_1$ pattern for CGpQ_0.50A. The main peak of anhydrite, $(\theta)/\lambda = 0.143$ Å^{-1}, is located at 25.4, 11.6 and 12.7° 2θ for Cu $K\alpha_1$, Mo $K\alpha_1$ and synchrotron radiations, respectively. The peak at $\sin(\theta)/\lambda = 0.1445$ Å^{-1} is due to the soluble anhydrite from gypsum (constant content in all the samples). The very tiny peak at $\sin(\theta)/\lambda = 0.1457$ Å^{-1}, which is slightly visible only in the SXRPD pattern, arises from $SrSO_4$ (0.39 wt%) from gypsum.

xylose, the ADP values were not reported in the original publications. Hence, they were obtained from the fits to the Mo $K\alpha_1$ patterns for the single phases. Three groups of isotropic ADPs were refined: those for O, C and H atoms. The final ADP values are given in León-Reina *et al.* (2016) as well as the R_F values before and after optimization, showing the improvements in the fits. For RQPA of all of the mixtures the ADPs were kept fixed.

Preferred orientation was modelled by the March–Dollase algorithm along the [001] axis for both glucose and lactose. Since microparticle sizes and distributions for different phases may